Letter

Gapless excitations inside the fully gapped kagome superconductors AV_3Sb_5

Yuhao Gu,[1,*] Yi Zhang,[2,3,*] Xilin Feng,[1,4] Kun Jiang,[1,†] and Jiangping Hu[1,3,‡]

[1]*Beijing National Laboratory for Condensed Matter Physics and Institute of Physics, Chinese Academy of Sciences, Beijing 100190, China*
[2]*Department of Physics, Shanghai University, Shanghai 200444, China*
[3]*Kavli Institute of Theoretical Sciences, University of Chinese Academy of Sciences, Beijing 100190, China*
[4]*School of Physical Sciences, University of Chinese Academy of Sciences, Beijing 100190, China*

(Received 22 September 2021; revised 18 January 2022; accepted 1 March 2022; published 17 March 2022)

The superconducting gap structures in the transition-metal-based kagome metal AV_3Sb_5 (A = K, Rb, Cs), the first family of quasi-two-dimensional kagome superconductors, remain elusive as there is strong experimental evidence for both nodal and nodeless gap structures. Here we show that the dichotomy can be resolved because of the coexistence of time-reversal symmetry breaking with a conventional fully gapped superconductivity. The symmetry protects the edge states which arise on the domains of the lattice symmetry breaking order to remain gapless in proximity to a conventional pairing. We demonstrate this result in a four-band tight-binding model using the V $d_{X^2a-Y^2}$-like and the in-plane Sb p_z-like Wannier functions that can faithfully capture the main feature of the materials near the Fermi level.

DOI: 10.1103/PhysRevB.105.L100502

Because of their unique lattice structure, kagome materials have become an important platform for studying the interplay between electron correlation, topology, and geometry frustration. Recently, the family of AV_3Sb_5 (A = K, Rb, Cs) materials has been found to be the first quasi-two-dimensional kagome superconductors (SCs) [1–11]. These materials display many very intriguing phenomena. For example, an unconventional charge density wave (CDW) order has been found in the nonmagnetic AV_3Sb_5 [1,2,12–14], which is also concurrent with the anomalous Hall effect (AHE) [15]. Muon spin spectroscopy (μSR) measurements [14,16–18] have revealed solid evidence for time-reversal symmetry breaking (TRSB). In order to explain the TRSB, many theories have been proposed [19–23]. In particular, the chiral flux phase (CFP) [19], which carries unique nontrivial topological properties, can naturally explain the TSRB and AHE.

For the superconducting properties of AV_3Sb_5, there are many controversial experimental results. On one hand, the superconductivity appears to be quite conventional. A Hebel-Slichter coherence peak appears just below the SC T_c from the spin-lattice relaxation measurement from the $^{121/123}$Sb nuclear quadrupole resonance [24]. The coherence peak is widely known as a hallmark for a conventional s-wave SC [25,26], which is also consistent with the decreasing Knight shift after the SC transition [24]. The magnetic penetration depth measurements also suggest a full gapped superconducting state for CsV_3Sb_5 [18,27]. There is also no magnetic resonance peak, which normally appears in superconductors with strong electron-electron correlation, such as cuprates and iron-based superconductors [28]. The weak electron-electron correlation in these materials is consistent with angle-resolved photoemission spectroscopy (ARPES) measurements [2,29–35] and the first-principle calculations [36,37]. In addition, the SC is very sensitive to magnetic impurities but without any resonance peaks to nonmagnetic impurities [38]. The μSR measurements also fail to detect any additional TRSB signals below T_c, which indicates a time-reversal persevered SC order parameter [18]. On the other hand, the thermoelectric transport measurements show a finite residual thermal conductivity at $T \to 0$ in CsV_3Sb_5, which indicates a nodal SC feature [5,39]. Scanning tunneling microscopy (STM) observes the V-shape density of states, which is a typical feature for gapless SCs [8,9,38]. As the existence of a gapless excitation normally indicates an unconventional superconductor, it is fundamentally important to find out a reconciliation of these experimental results.

In this Letter, we suggest that because of the existence of TRSB, the gapless topological edge states are forbidden by symmetry from opening a gap by pairing in proximity to a conventional pairing. Thus, those gapless states on the domains of the CDW or hidden orders remain gapless in the superconducting states. Specifically, there are two key discrete symmetries in SCs to guarantee the presence of Cooper pairing, time-reversal T, and inversion symmetry I [40–42]. Since the T maps a $|k,\uparrow\rangle$ state to $|-k,\downarrow\rangle$ state, the system at least contains time-reversal symmetry for the even-parity spin-singlet pairing formed by $(c_{k,\uparrow}c_{-k,\downarrow} - c_{k,\downarrow}c_{-k,\uparrow})$, as illustrated in Fig. 1(a). In the same spirit, the odd-parity spin-triplet pairing needs inversion symmetry I owing to the fact that I maps a $|k,\uparrow\rangle$ state to $|-k,\uparrow\rangle$ state, as illustrated in Fig. 1(b). These two symmetry conditions are known as the Anderson theorem [40–42]. For AV_3Sb_5 SC cases, due to TRSB, the normal states before the SC transition breaks the T symmetry. Therefore, the edge modes on CDW

*These authors contributed equally to this work.
†jiangkun@iphy.ac.cn
‡jphu@iphy.ac.cn

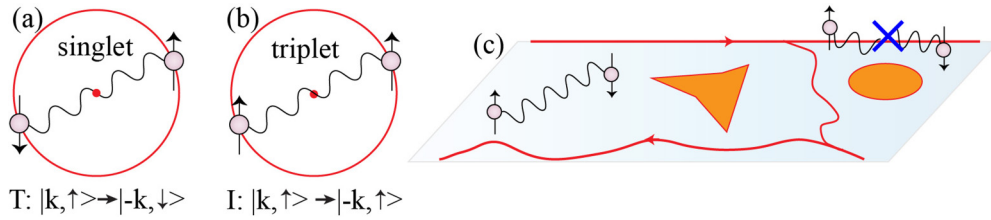

FIG. 1. (a) The time-reversal operator T maps a $|k,\uparrow\rangle$ state to $|-k,\downarrow\rangle$ state, which is the essential symmetry for spin-singlet Cooper pairs. (b) The inversion operator I maps a $|k,\uparrow\rangle$ state to $|-k,\uparrow\rangle$ state, which is the essential symmetry for spin-triplet Cooper pairs. (c) The edge states, CDW domain walls, and other crystal grain boundaries, etc., are not gapped out by the SC pairings.

domain walls which break the T symmetry or other crystal grain boundaries cannot be gapped out by the SC, as illustrated in Fig. 1(c). Hence, although the AV_3Sb_5 SC can be a conventional s wave, it still contains gapless excitations. To demonstrate this physics, we construct a four-band tight-binding (TB) model, which faithfully captures the band structures of AV_3Sb_5 near Fermi energy. Since the inversion symmetry is always a good symmetry for AV_3Sb_5 normal state from the recent second-harmonic generation measurement [17], the spin-singlet pairing and spin-triplet pairing should be separated. We will focus on the spin singlet in this work based on the decreasing Knight shift from NMR [24].

Since all AV_3Sb_5 materials have very similar band structures, we take CsV_3Sb_5 as an example. From the density functional theory (DFT) calculations and ARPES measurements [2,29], there are multibands crossing the Fermi level, as shown in Fig. 2(a). The crystal structure of CsV_3Sb_5 is shown in Figs. 2(b) and 2(c). The DFT and ARPES results

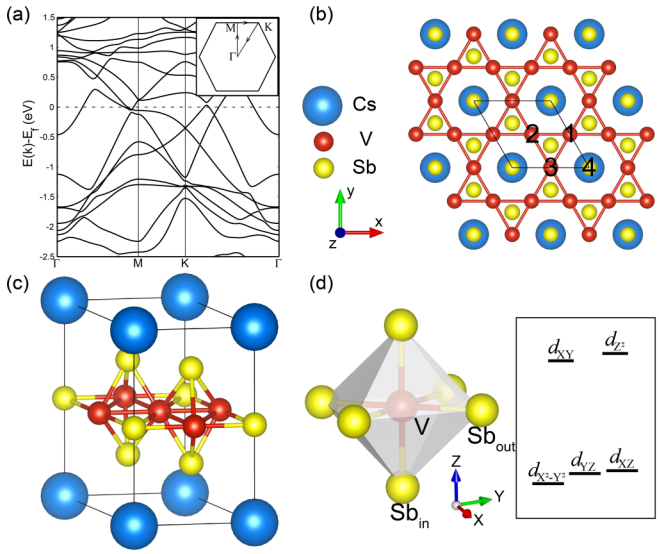

FIG. 2. (a) Band structure of CsV_3Sb_5 from DFT calculation with SOC. The inset shows the high symmetry **k** path we use. (b) Crystal structure of CsV_3Sb_5 from the top view. The Wannier centers of Wannier functions in the TB model are labeled as 1–4. (c) Crystal structure of CsV_3Sb_5 from another angle view. (d) The illustration of the VSb_6 octahedra complex under the local coordinate (X-Y-Z) and the schematic illustration for the crystal field splitting under this local coordinate. There are two types of Sb atoms: two Sb atoms are in the same plane with V atoms while the other four Sb atoms are out of plane.

show that AV_3Sb_5 is a quasi-two-dimensional metal, whose electronic physics is dominated by electrons from the V-Sb plane [1,2,29]. In this V-Sb plane, three V atoms form a kagome lattice and an additional Sb atom forms a triangle lattice locating at the V hexagonal center. Above and below this V-Sb plane, out-of-plane Sb atoms form two honeycomb lattices, respectively. Cs atoms form another triangle lattice above or below these Sb honeycomb planes.

We will show that a four-band TB model can faithfully capture the main physics behind AV_3Sb_5 based on Wannierization and symmetry analysis. To understand the band structure, we first focus on the local atomic structure of V atoms. There are three V atoms in the kagome lattice's unit cell [labeled as 1–3, as indicated in Fig. 2(b)] and here we choose the local coordinate (X-Y-Z) for each site, as shown in Fig. 2(d). Let us take V-3 as an example to explain the definition of the local coordinate: as the global coordinate changes to the local coordinate, the axis x-y-z turns to Z-X-Y on V-3. By using C_3 symmetric operation, we can get the other two local coordinates on V-1 and V-2. In the local symmetric coordinate, the Z axis always points to the in-plane Sb atom and the Y axis is same as the z axis in the global x-y-z coordinate. The V atom can be considered as being coordinated in a distorted octahedron, whose point group symmetry is D_{2h}. The D_{2h} crystal field leads to no degeneracies of all the five d orbitals [Fig. 2(d)], consistent with our Wannierization result in the Supplemental Material [43] (see, also, references [44–48] therein). In the local coordinate, the energy of the d_{XY}/d_{Z^2} orbital is higher than that of the $d_{X^2-Y^2}$-d_{XZ}-d_{YZ} orbital, similar to the familiar e_g-t_{2g} relationship in a nondistorted octahedral crystal field.

From the DFT calculation and Wannierization, we find that the eigenstate of the von Hove (vH) point is mainly from the local $d_{X^2-Y^2}$ orbital discussed above. More importantly, the $d_{X^2-Y^2}$ orbital of this vH is dominated by the single V sublattice. This feature is the reason why a single orbital model on kagome lattice is a reasonable starting model for these materials [23,49–51]. Namely, a minimal TB model based on the local $d_{X^2-Y^2}$ orbitals can capture the main physics of AV_3Sb_5, especially the vH around the Fermi level. Besides the V d orbital, there is one additional electron pocket around the Γ point, which is attributed to the in-plane Sb's p_z orbital. Without the spin-orbital coupling (SOC), there is no overlap between the in-plane Sb p_z orbital and the V $d_{X^2-Y^2}$ orbital. Hence, the p_z band can be isolated from V $d_{X^2-Y^2}$ bands.

Based on the above observation, we apply the maximally localized Wannier functions method to get the minimal model for CsV_3Sb_5. Using the local V-centered $d_{X^2-Y^2}$-like Wannier function, a three-band model on the kagome lattice is obtained

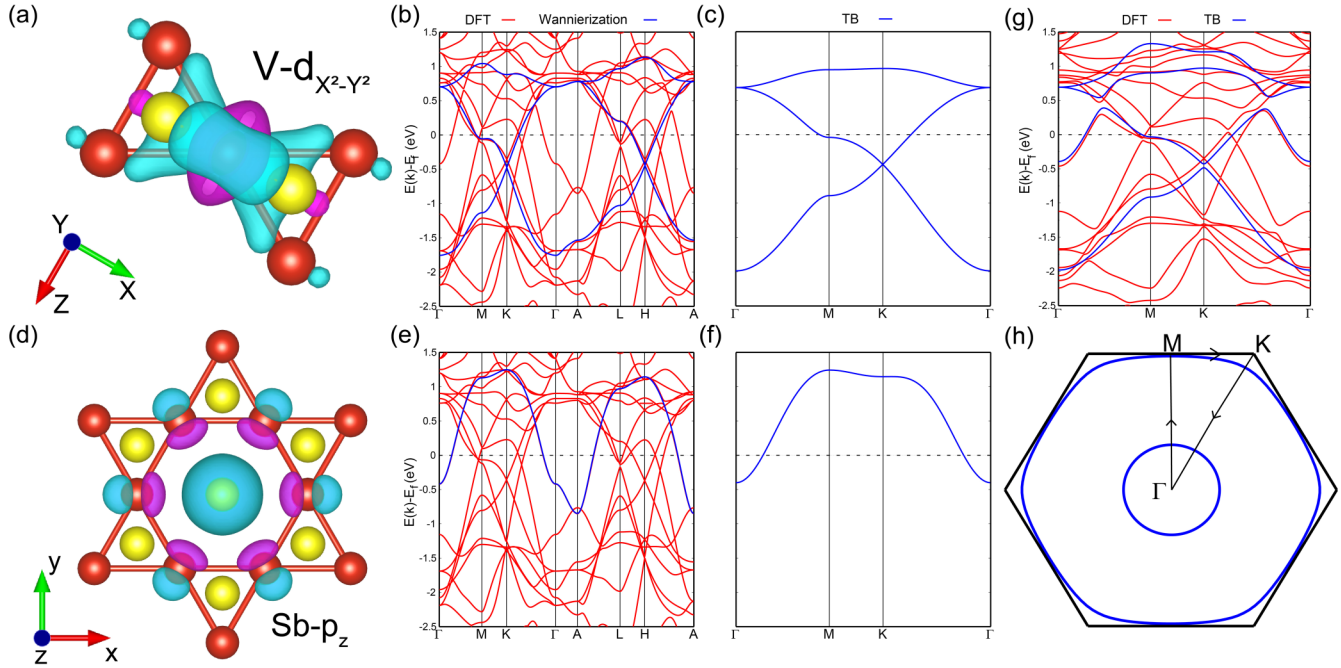

FIG. 3. (a) The $d_{X^2-Y^2}$-like Wannier function on the V atom under the local X-Y-Z coordinate. The other two $d_{X^2-Y^2}$-like Wannier functions are symmetric. (b) Band structures of CsV_3Sb_5 from DFT and Wannierization of three $d_{X^2-Y^2}$-like Wannier functions without SOC. (c) Band structure of the TB model with three $d_{X^2-Y^2}$-like Wannier functions. (d) The p_z-like Wannier function on the in-plane Sb atom under the global x-y-z coordinate. (e) Band structures of CsV_3Sb_5 from DFT and Wannierization of the p_z-like Wannier function without SOC. (f) Band structure of the TB model with the p_z-like Wannier function. (g) Band structure of the TB model with SOC. (h) The Fermi surface of the TB model.

as shown in Fig. 3(b). The corresponding Wannier function is also plotted in Fig. 3(a). By comparing with the DFT results in Fig. 3(b), we find this three-band model well describes the main feature of vH points around the Fermi level and the Dirac cone at the K points. Additionally, using the in-plane–Sb-centered p_z-like Wanner function, a single p_z band on triangle lattice is also obtained, as plotted in Fig. 3(e). Its Wannier function is also shown in Fig. 3(d). As shown in Fig. 3(e), the Wannierized p_z band exactly agrees with the DFT calculation. Hence, the p_z band is isolated from other bands without SOC as discussed above. The SOC coupling terms can be further added in the minimal model using point group symmetry [43].

The effective TB model in the basis of three symmetric $d_{X^2-Y^2}$-like Wannier functions (labeled as 1–3) and one p_z-like Wannier function (labeled as 4) to describe the in-plane electronic physics, as shown in Fig. 3(g). Including the SOC, the TB Hamiltonian can be written as

$$H_{\mathrm{TB}} = H_{\mathrm{V}} + H_{\mathrm{Sb}} + H_{\mathrm{SOC}}. \tag{1}$$

Details of this Hamiltonian with SOC can be found in the Supplemental Material [43] (see, also, references [44–48] therein).

Motivated by the chiral CDW found by magnetic-field dependent STM measurements [14] and its concurrence with AHE [15], several TRSB flux states have been proposed to explain the phenomena [19–23]. Among them, the lowest energy CFP as shown in Fig. 4(a) [19,23] has gained support from recent μSR measurements [16,17]. In the single orbital model, the CFP state has $C = 2$ Chern number [19]. The topological aspects of the CFP state in the minimal model

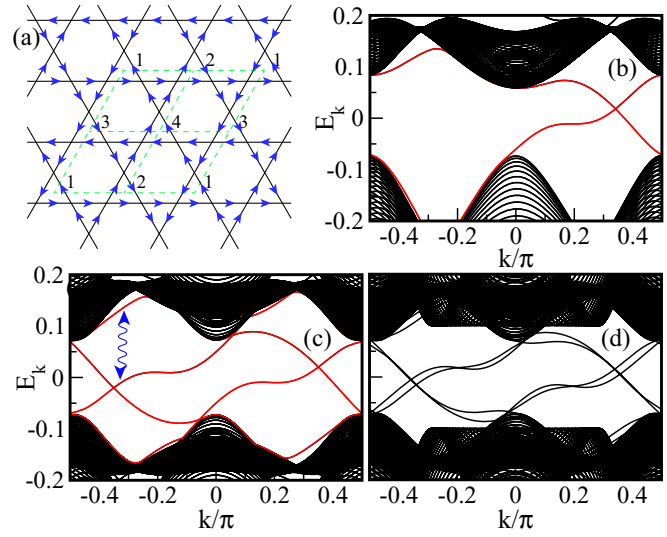

FIG. 4. (a) The hopping flux configuration for the chiral flux phase. (b) The edge states spectrum for the chiral flux phase without Sb bands. (c) The BdG spectrum for the pairing state without Sb bands. The energy difference δ_E between $E_{k,\uparrow}$ and $E_{-k,\downarrow}$ is on the order of Δ_{CFP}. (d) The BdG spectrum for the pairing state with Sb bands, where the SOC splits the in-gap bands. Here we take the CFP order parameter $\Delta_{\mathrm{CFP}} = 0.2$ eV and the on-site pairing for both V and Sb atoms to be $\Delta_{\mathrm{SC}} = 0.1$ eV and the chemical potential $\mu = -0.1$ eV. For the edge state calculation, we consider a system with translation invariance along the $\mathbf{a}_1$ direction and open boundary condition along the $\mathbf{a}_2$ direction with length of 100 lattice constant.

remains the same as before. To confirm this, we carry out an open boundary calculation for the minimal model coupling with the CFP order. Note that we have ignored the Sb bands to avoid the complication. As shown in Fig. 4(b), there are chiral edge states from nonzero Chern number inside the bulk gap. It is important to point out that due to TRSB and inversion symmetry breaking at the boundary, the edge state spectrum has no relation between $\mathbf{k}$ and $-\mathbf{k}$ anymore.

Now, we consider superconductivity in this system. The standard Bogoliubov–de Gennes (BdG) Hamiltonian can be written as

$$H_{\mathrm{BdG}} = \begin{pmatrix} H_{\mathrm{TB}}(k) - \mu & \hat{\mathbf{\Delta}}(\mathbf{r}) \\ \hat{\mathbf{\Delta}}^{\dagger}(\mathbf{r}) & -H_{\mathrm{TB}}^{T}(-k) + \mu \end{pmatrix}, \tag{2}$$

in the basis $\Psi_k = (c_{k\uparrow}, c_{k\downarrow}, c^{\dagger}_{-k\uparrow}, c^{\dagger}_{-k\downarrow})^T$, where μ is the chemical potential and $\hat{\mathbf{\Delta}}(\mathbf{r})$ is the pairing function. We consider a standard s-wave function, $\hat{\mathbf{\Delta}}(\mathbf{r}) = \mathbf{\Delta}(\mathbf{r}) i s_y$ with s_y the corresponding Pauli matrix in the spin space. Since our symmetry analysis and discussion does not depend on details of the microscopic model, we take the on-site s-wave pairing as an example, namely, $\mathbf{\Delta}(\mathbf{r}) = \Delta_{\mathrm{SC}}$. As shown in Fig. 4(c), the edge states remain gapless after the SC order is introduced. From Figs. 4(b) and 4(c), we can find that the energy difference δE between $E_{k,\uparrow}$ of the $|k, \uparrow\rangle$ state and $E_{-k,\downarrow}$ of the $|-k, \downarrow\rangle$ state is on the order of the TRSB gap Δ_{CFP}. Therefore, if the pairing gap Δ_{SC} is much smaller than δE, the edge states are always gapless. This result is still valid if we include the Sb band and the SOC term in the above calculation, as shown in Fig. 4(d).

Experimentally, Δ_{CFP} is much larger than the Δ_{SC} in this family of materials. The μSR measurements show that the TRSB starts around $T \approx 70$ K for CsV_3Sb_5 with the CDW transition temperature $T \approx 90$ K [17]. The SC transition temperature is much smaller with $T_c \approx 2.5$ K [2]. Hence, regardless of the microscopic pairing form, we expect that there are always gapless excitations in the edges, domain walls, and other places of AV_3Sb_5 SC, where the TRSB order plays a dominant role. This result can explain the residual thermal conductivity, where the gapless excitations contribute thermal conductivity like the conventional electrons. It is clear that the above result can be extended to the spin-triplet pairing bulk state. In this case, the topological gapless states at the inversion symmetry broken structures can remain gapless.

In summary, we conclude that the AV_3Sb_5 ground state contains gapless excitations owing to its TRSB normal state even if the bulk superconductivity is fully gapped. To confirm this, a four-band TB model is constructed to capture electronic band structures of the materials, using the V-centered $d_{X^2\text{-}Y^2}$ -like Wannier functions and the in-plane Sb-centered p_z-like Wannier function based on the technique of Wannierization and symmetry analysis. In this case, topological gapless excitations due to the TRSB remain gapless when a fully gapped SC order parameter is induced. Our proposal can be justified or falsified easily by measuring the states on edges or domain boundaries.

We thank S. Li, L. Yu, and J. Yin for useful discussions. This work is supported by the Ministry of Science and Technology (Grant No. 2017YFA0303100), National Science Foundation of China (Grants No. NSFC-11888101 and No. NSFC-12174428), and the Strategic Priority Research Program of Chinese Academy of Sciences (Grant No. XDB28000000). K.J. acknowledges support from the start-up grant of IOP-CAS. Y.Z. is supported in part by NSF China Grants No. 12004383 and No. 12074276 and the Fundamental Research Funds for the Central Universities.

The authors declare no conflict of interest.

[1] B. R. Ortiz, L. C. Gomes, J. R. Morey, M. Winiarski, M. Bordelon, J. S. Mangum, I. W. H. Oswald, J. A. Rodriguez-Rivera, J. R. Neilson, S. D. Wilson *et al.*, Phys. Rev. Materials **3**, 094407 (2019).

[2] B. R. Ortiz, S. M. L. Teicher, Y. Hu, J. L. Zuo, P. M. Sarte, E. C. Schueller, A. M. Milinda Abeykoon, M. J. Krogstad, S. Rosenkranz, R. Osborn *et al.*, Phys. Rev. Lett. **125**, 247002 (2020).

[3] B. R. Ortiz, P. M. Sarte, E. M. Kenney, M. J. Graf, S. M. L. Teicher, R. Seshadri, and S. D. Wilson, Phys. Rev. Materials **5**, 034801 (2021).

[4] Q. Yin, Z. Tu, C. Gong, Y. Fu, S. Yan, and H. Lei, Chin. Phys. Lett. **38**, 037403 (2021).

[5] C. C. Zhao, L. S. Wang, W. Xia, Q. W. Yin, J. M. Ni, Y. Y. Huang, C. P. Tu, Z. C. Tao, Z. J. Tu, C. S. Gong *et al.*, arXiv:2102.08356.

[6] F. Du, S. Luo, B. R. Ortiz, Y. Chen, W. Duan, D. Zhang, X. Lu, S. D. Wilson, Y. Song, and H. Yuan, Phys. Rev. B **103**, L220504 (2021).

[7] K. Y. Chen, N. N. Wang, Q. W. Yin, Y. H. Gu, K. Jiang, Z. J. Tu, C. S. Gong, Y. Uwatoko, J. P. Sun, H. C. Lei *et al.*, Phys. Rev. Lett. **126**, 247001 (2021).

[8] Z. Liang, X. Hou, F. Zhang, W. Ma, P. Wu, Z. Zhang, F. Yu, J.-J. Ying, K. Jiang, L. Shan *et al.*, Phys. Rev. X **11**, 031026 (2021).

[9] H. Chen, H. Yang, B. Hu, Z. Zhao, J. Yuan, Y. Xing, G. Qian, Z. Huang, G. Li, Y. Ye *et al.*, Nature (London) **599**, 222 (2021).

[10] X. Chen, X. Zhan, X. Wang, J. Deng, X.-B. Liu, X. Chen, J.-G. Guo, and X. Chen, Chin. Phys. Lett. **38**, 057402 (2021).

[11] S. Ni, S. Ma, Y. Zhang, J. Yuan, H. Yang, Z. Lu, N. Wang, J. Sun, Z. Zhao, D. Li *et al.*, Chin. Phys. Lett. **38**, 057403 (2021).

[12] Y.-P. Lin and R. M. Nandkishore, arXiv:2107.09050.

[13] E. M. Kenney, B. R. Ortiz, C. Wang, S. D. Wilson, and M. J. Graf, J. Phys.: Condens. Matter **33**, 235801 (2021).

[14] Y.-X. Jiang, J.-X. Yin, M. M. Denner, N. Shumiya, B. R. Ortiz, G. Xu, Z. Guguchia, J. He, M. S. Hossain, X. Liu *et al.*, Nat. Mater. **20**, 1353 (2021).

[15] F. H. Yu, T. Wu, Z. Y. Wang, B. Lei, W. Z. Zhuo, J. J. Ying, and X. H. Chen, Phys. Rev. B **104**, L041103 (2021).

[16] C. Mielke III, D. Das, J.-X. Yin, H. Liu, R. Gupta, C. Wang, Y.-X. Jiang, M. Medarde, X. Wu, H. Lei *et al.*, Nature (London) **602**, 245 (2022)

[17] L. Yu, C. Wang, Y. Zhang, M. Sander, S. Ni, Z. Lu, S. Ma, Z. Wang, Z. Zhao, H. Chen *et al.*, arXiv:2107.10714.

[18] R. Gupta, D. Das, C. H. Mielke III, Z. Guguchia, T. Shiroka, C. Baines, M. Bartkowiak, H. Luetkens, R. Khasanov, Q. Yin *et al.*, arXiv:2108.01574.
[19] X. Feng, K. Jiang, Z. Wang, and J. Hu, Sci. Bull. **66**, 1384 (2021).
[20] M. M. Denner, R. Thomale, and T. Neupert, Phys. Rev. Lett. **127**, 217601 (2021).
[21] Y.-P. Lin and R. M. Nandkishore, Phys. Rev. B **104**, 045122 (2021).
[22] T. Park, M. Ye, and L. Balents, Phys. Rev. B **104**, 035142 (2021).
[23] X. Feng, Y. Zhang, K. Jiang, and J. Hu, Phys. Rev. B **104**, 165136 (2021).
[24] C. Mu, Q. Yin, Z. Tu, C. Gong, H. Lei, Z. Li, and J. Luo, Chin. Phys. Lett. **38**, 077402 (2021).
[25] L. C. Hebel and C. P. Slichter, Phys. Rev. **107**, 901 (1957).
[26] L. C. Hebel and C. P. Slichter, Phys. Rev. **113**, 1504 (1959).
[27] W. Duan, Z. Nie, S. Luo, F. Yu, B. R. Ortiz, L. Yin, H. Su, F. Du, A. Wang, Y. Chen *et al.*, Sci. China Phys. Mech. Astron. **64**, 107462 (2021).
[28] D. J. Scalapino, Rev. Mod. Phys. **84**, 1383 (2012).
[29] H. Luo, Q. Gao, H. Liu, Y. Gu, D. Wu, C. Yi, J. Jia, S. Wu, X. Luo, Y. Xu *et al.*, Nat. Commun. **13**, 273 (2022).
[30] H. X. Li, T. T. Zhang, Y. Y. Pai, C. Marvinney, A. Said, Q. Yin, C. Gong, Z. Tu, E. Vescovo *et al.*, Phys. Rev. X **11**, 031050 (2021).
[31] Z. Wang, S. Ma, Y. Zhang, H. Yang, Z. Zhao, Y. Ou, Y. Zhu, S. Ni, Z. Lu, H. Chen *et al.*, arXiv:2104.05556.
[32] K. Nakayama, Y. Li, T. Kato, M. Liu, Z. Wang, T. Takahashi, Y. Yao, and T. Sato, Phys. Rev. B **104**, L161112 (2021).
[33] Y. Luo, S. Peng, S. M. L. Teicher, L. Huai, Y. Hu, B. R. Ortiz, Z. Wei, J. Shen, Z. Ou, B. Wang *et al.*, arXiv:2106.01248.
[34] Z. Liu, N. Zhao, Q. Yin, C. Gong, Z. Tu, M. Li, W. Song, Z. Liu, D. Shen, Y. Huang *et al.*, Phys. Rev. X **11**, 041010 (2021).
[35] Y. Hu, S. M. L. Teicher, B. R. Ortiz, Y. Luo, S. Peng, L. Huai, J. Z. Ma, N. C. Plumb, S. D. Wilson, J. F. He, and M. Shi, Sci. Bull. **67**, 495 (2022).
[36] J.-F. Zhang, K. Liu, and Z.-Y. Lu, Phys. Rev. B **104**, 195130 (2021).
[37] J. Zhao, W. Wu, Y. Wang, and S. A. Yang, Phys. Rev. B **103**, L241117 (2021).
[38] H.-S. Xu, Y.-J. Yan, R. Yin, W. Xia, S. Fang, Z. Chen, Y. Li, W. Yang, Y. Guo, and D.-L. Feng, Phys. Rev. Lett. **127**, 187004 (2021).
[39] X. Wu, T. Schwemmer, T. Muller, A. Consiglio, G. Sangiovanni, D. Di Sante, Y. Iqbal, W. Hanke, A. P. Schnyder, M. M. Denner *et al.*, Phys. Rev. Lett. **127**, 177001 (2021).
[40] P. W. Anderson, J. Phys. Chem. Solids **11**, 26 (1959).
[41] P. W. Anderson, Phys. Rev. B **30**, 4000 (1984).
[42] M. Sigrist, *Introduction to Unconventional Superconductivity in Non-Centrosymmetric Metals*, AIP Conf. Proc. No. 1162 (AIP, Melville, NY, 2009), p. 55.
[43] See Supplemental Material at http://link.aps.org/supplemental/10.1103/PhysRevB.105.L100502 for more detailed discussions.
[44] G. Kresse and J. Furthmüller, Phys. Rev. B **54**, 11169 (1996).
[45] G. Kresse and D. Joubert, Phys. Rev. B **59**, 1758 (1999).
[46] J. P. Perdew, K. Burke, and M. Ernzerhof, Phys. Rev. Lett. **77**, 3865 (1996).
[47] A. A. Mostofi, J. R. Yates, Y.-S. Lee, I. Souza, D. Vanderbilt, and N. Marzari, Comput. Phys. Commun. **178**, 685 (2008).
[48] Y. Gu, X. Wu, K. Jiang, and J. Hu, Chin. Phys. Lett. **38**, 017501 (2021).
[49] S.-L. Yu and J.-X. Li, Phys. Rev. B **85**, 144402 (2012).
[50] W.-S. Wang, Z.-Z. Li, Y.-Y. Xiang, and Q.-H. Wang, Phys. Rev. B **87**, 115135 (2013).
[51] M. L. Kiesel, C. Platt, and R. Thomale, Phys. Rev. Lett. **110**, 126405 (2013).